Numerical Modeling of Space Plasma Flows: ASTRONUM-2014
ASP Conference Series, Vol. 498
N. V. Pogorelov, E. Audit, and G. P. Zank, eds.

Vlasiator: Global Kinetic Magnetospheric Modeling Tool

A. Sandroos,[1,2] S. von Alfthan,[1] S. Hoilijoki,[1,3] I. Honkonen,[4] Y. Kempf,[1,3]
D. Pokhotelov,[5] and M. Palmroth[1]

[1]*Finnish Meteorological Institute, P.O.Box 503, FI-00101 Helsinki, Finland*
[2]*Space Sciences Laboratory, University of California, Berkeley, CA, USA*
[3]*University of Helsinki, Helsinki, Finland*
[4]*NASA Goddard Space Flight Center, Greenbelt, MD, USA*
[5]*Mullard Space Science Laboratory, University College London, UK*

Abstract. We present Vlasiator, a novel code based on Vlasov's equation, developed for modeling magnetospheric plasma on a global scale. We have parallelized the code to petascale supercomputers with a hybrid OpenMP-MPI approach to answer the high computational cost of propagating ion distribution functions in six dimensions. The accuracy of the numerical method is demonstrated by comparing simulated wave dispersion plots to analytical results. Simulations of Earth's bow shock region were able to reproduce many well-known plasma phenomena, such as compressional magnetosonic waves in the foreshock region, and mirror mode instability in the magnetosheath.

1. Introduction

Space weather attempts to predict conditions in near-Earth space that can cause harm to humans or technological systems. Major space weather events are driven by coronal mass ejections which, upon impacting Earth's magnetosphere, can for example cause errors in GPS positioning, overload transformers via geomagnetically induced currents, or cause system failure on satellites used by TV companies. Accurate space weather prediction, requiring capability to model the whole system from the solar surface to inside Earth's crust, is still beyond reach. However, many important effects can be captured by just modeling the magnetosphere and the immediate interplanetary space.

First global models of Earth's magnetosphere, such as Finnish Meteorological Institute's GUMICS-4 (Janhunen et al. 2012), were based on ideal MHD models and have been successful in modeling systems where the plasma can be described with a single temperature. This leaves out important physical phenomena, such as magnetic reconnection, or magnetospheric regions such as ion foreshock or ring current, where the plasma has multiple components.

Currently two approaches are being used in an attempt to improve the global models. The first one is based on coupling dedicated models together (e.g., Daldorff et al. 2014), which may be faster if the dedicated models already exist. However, interface between models based on different sets of equations may be problematic. A more fundamental approach is to use a kinetic description for the whole system, e.g., by modeling the whole system by using a full particle simulation (e.g., Savoini et al. 2013), or use a model based on Vlasov's equation like in the Vlasiator code. The downside of fully kinetic models is the extremely high computational cost. We have previously modeled the magnetosphere by using a test-Vlasov solver (Palmroth et al. 2013).

This manuscript gives an overview of Vlasiator, starting with a description of the numerical approach. We then discuss aspects related to the parallel implemention that were necessary to scale the code to petascale supercomputers. Finally, we present results from self-consistent simulations.

2. Numerical Method

A fundamental description of a collisionless plasma is given by the Vlasov equation

$$\partial_t f + (\mathbf{v}\cdot\nabla_r) f + (\mathbf{a}\cdot\nabla_v) f = 0 \tag{1}$$

for ion distribution function $f = f(\mathbf{r},\mathbf{v},t)$. Here $\mathbf{r}$ and $\mathbf{v}$ are the coordinates in spatial and velocity directions, $\mathbf{a} = (q/m)(\mathbf{E}+\mathbf{v}\times\mathbf{B})$ is the Lorentz force, and q and m are the ion charge and mass. Convectional electric field is supplemented by a Hall term,

$$\mathbf{E} = -\mathbf{V}\times\mathbf{B} + (\mathbf{j}\times\mathbf{B})/\rho_q, \tag{2}$$

where the ion charge density ρ_q and bulk velocity $\mathbf{V}$ are obtained as moments of f,

$$\rho_q = q\int f\, d^3v, \quad \mathbf{V} = \left(q/\rho_q\right)\int \mathbf{v} f\, d^3v. \tag{3}$$

In self-consistent models the Vlasov equation is coupled with Maxwell's equations,

$$\nabla\cdot\mathbf{E} = 0,\ \nabla\cdot\mathbf{B} = 0,\ \nabla\times\mathbf{E} = -\partial_t\mathbf{B},\ \nabla\times\mathbf{B} = \mu_0\mathbf{j}, \tag{4}$$

where quasi-neutrality is assumed and displacement current is neglected in Ampère–Maxwell's law. Vlasov's equation is just an advection equation for a six-dimensional fluid. We write equation (1) in conservative form,

$$\partial_t F + \nabla\cdot(\mathbf{v}F) + \nabla\cdot(\mathbf{a}F) = 0, \tag{5}$$

and use a finite volume method to propagate phase-space averages of f,

$$F = \int_{\text{cell}} f/\left(\Delta^3 r\Delta^3 v\right) d^3r\, d^3v, \tag{6}$$

where $\Delta^3 r$ and $\Delta^3 v$ are the cell volumes in spatial and velocity dimensions (Leveque 1997; Langseth & Leveque 2000).

The fluxes in equation (5) are simply

$$H_r = \mathbf{v}F, \quad H_v = (q/m)\left(\mathbf{v}-\mathbf{V}+\mathbf{j}/\rho_q\right)\times\mathbf{B}\,F. \tag{7}$$

Phase-space averages are then propagated as

$$F(t+\Delta t) = F(t) - \underbrace{\frac{\Delta t}{\Delta x}\left[H_x^{i+1} - H_x^{i}\right]}_{\text{translation } S_T(\Delta t)} - \cdots - \underbrace{\frac{\Delta t}{\Delta vz}\left[H_{vz}^{n+1} - H_{vz}^{n}\right]}_{\text{acceleration } S_A(\Delta t)}, \tag{8}$$

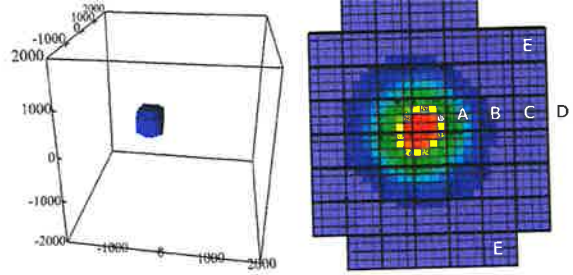

Figure 1. (*Left panel*) The distribution function of solar wind is concentrated near its bulk velocity, and most of the velocity mesh is empty. (*Right panel*) Illustration of the sparse velocity mesh. Blocks marked with A and B are flagged as blocks with content. Block C is a stored no-content block neighboring a block with content. Block D is not stored. Blocks E are stored because they have spatial neighbors with content.

where (i, j, k, l, m, n) are the six cell indices. We split Eqn. (8) into separate 3D propagation steps using Strang splitting, $F(t+\Delta t) = S_T(\Delta t/2)S_A(\Delta t)S_T(\Delta t/2)\,F(t)$. Translation operators can be combined to save computation time, i.e., translation and acceleration are leap-frogged over interleaved time steps. The solution can be synchronized in **r** and **v** by applying $S_T(\Delta t/2)$ to translate the solution forward in time whenever needed.

The magnetic field is propagated by using a constrained transport scheme (Londrillo & del Zanna 2004), and a second-order accurate Runge–Kutta propagator. Integral form of Fadaray's law is used to propagate **B,** defined by its normal components averaged over cell faces, forward in time. Components of **E**, averaged over cell edges, are needed. We reconstruct the values by using formulas given in Balsara et al. (2009) to interpolate ρ_q, **V**, and **B** in Eqn. (2) to cell edges, and then calculate the edge averages.

Full propagation algorithm has three Courant–Friedrichs–Lewy (CFL) stability conditions for the simulation time step coming from S_T and S_A operators, and field solver. The CFL condition states that information propagating at speed u must not cross multiple spatial cells during one time step, $u\,\Delta t \leqslant \Delta x$. Usually the most stringent limitation comes from S_A operator, which we sub-step as necessary to keep simulation time step reasonable ($\sim$ 50 ms).

3. Parallelization Strategy

Vlasov simulations on magnetospheric scale are computationally very demanding. Typically we need few hundred cells per spatial dimension, i.e., roughly 10^6 (10^9) cells for two (three) dimensional runs. In velocity dimensions limits $\pm$2000 km/s are used to prevent distributions from flowing out of boundaries, and a 20 km/s grid resolution is used to keep numerical diffusion tolerable. Assuming a few thousand time steps, global scale runs require approximately 10^{18} phase-space cell propagations.

Vlasiator has been parallelized to large petascale supercomputers by using a hybrid MPI-OpenMP approach. The DCCRG library (Honkonen et al. 2013) is used to decompose the spatial mesh to computing nodes using MPI. Each spatial cell contains a velocity mesh, which is further divided into 4x4x4 Cartesian blocks, for storing the distribution function. All computations on a single node are multithreaded with OpenMP.

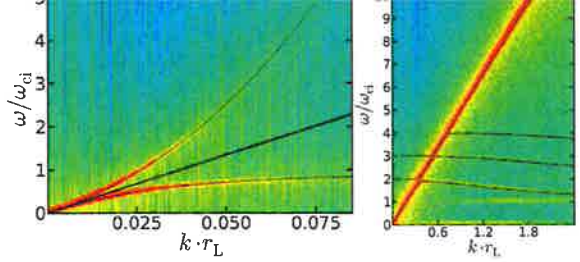

Figure 2. (*Left panel.*) Wave dispersion plot for quasi-parallel propagation from Vlasiator vs. analytical results. Shown are shear Alfvén wave (oblique line), and right- and left-hand polarized modes (upper and lower branches, correspondingly). The left-hand polarized mode has a cut-off at ion gyro frequency. (*Right panel.*) Dispersion plot for quasi-perpendicular propagation vs. WHAMP solutions. Strong oblique mode is the non-dispersive magnetosonic wave. First few Bernstein modes are visible but weak. Reprinted with permission from Kempf et al. (2013). Copyright 2013, AIP Publishing LLC.

Computational load can be considerably reduced by noting that the distribution functions are very localized in many regions (von Alfthan et al. 2014). For example, the slow solar wind is concentrated near $v_x \approx 450$ km/s. We only store velocity blocks where the value of F exceeds a pre-set threshold F_0 (blocks with content). Additionally, we store all 26 velocity space neighbors of content blocks, all 26 nearest neighbors in spatial directions, and second-nearest spatial neighbors in face-normal directions (Sandroos et al. 2013). Thus, a block can have $F < F_0$ but exist because it is a neighbor of a content block. If a no-content block accumulates enough material so that $F \geqslant F_0$, it becomes a content block and its neighbors are created. Conversely, no-content blocks are removed if all their neighbors are also no-content blocks (see Fig. 1).

Due to varying numbers of velocity blocks per cell, and substepping of S_A operator, propagation times of spatial cells can vary by a large factor. The mesh partitioner assigns very few computationally expensive cells to a node. The main benefit of using OpenMP threading is that it allows the code to scale to less than one spatial cell per core. Multithreading also reduces the number of MPI processes, i.e., more cells are assigned per process than in a pure MPI implementation. This can significantly reduce the data nodes exchange each time step (whole velocity mesh per spatial cell).

4. Results: Dispersion Relation

In ideal MHD, the only possible electromagnetic wave modes are the non-compressional shear Alfvén wave, and compressional fast and slow magnetosonic waves. Shear Alfvén waves do not propagate perpendicular to the mean **B**. Dispersion relations are

$$\left(\frac{\omega}{k}\right)^2 = \begin{cases} V_A^2 \cos^2\theta, & \text{shear waves} \\ \frac{1}{2}\left(V_A + V_s\right)^2 \pm \frac{1}{2}\sqrt{\left(V_A + V_s\right)^2 - 4V_A^2 V_s^2 \cos^2\theta}, & \frac{\text{fast}}{\text{slow}} \text{ magnetosonic} \end{cases} \tag{9}$$

where V_A and V_s are the Alfvń and sound speeds, and $\cos\theta = \mathbf{k}\cdot\mathbf{B}/(kB)$. Kinetic theories allow for more wave modes. Left- and right-handed polarized modes propagate

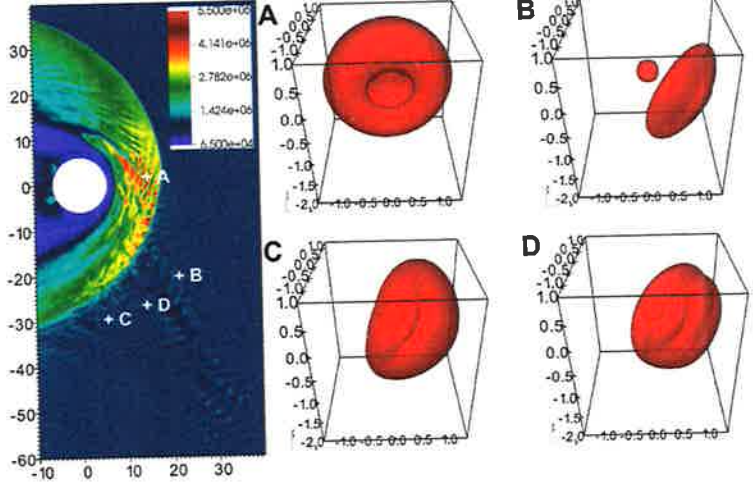

Figure 3. Plasma number density (in m^{-3}) at the end of a 2D magnetospheric run (coordinates in R_E). Quasi-parallel bow shock region reflects solar wind ions, and a foreshock associated with magnetosonic perturbations is formed. Magnetosheath, the region downstream of the bow shock, is characterized by perturbations driven by mirror mode instability. The panels on the right show the shapes of distribution functions at the positions marked with letters A-D.

along or quasi-parallel to mean **B** and, in low frequency limit, converge to the shear Alfvén wave. Last wave modes in range of interesting frequencies are the electrostatic ion Bernstein modes, quasi-perpendicular to the mean **B**.

Vlasiator wave dispersion plots were studied by using a periodic one-dimensional simulation box in x-direction (Kempf et al. 2013). Wave vectors were also constrained to lie in that direction. Angle between mean magnetic field and wave vector was defined by setting ambient **B** to be at an angle with respect to x-axis. Initially random perturbations were added to otherwise uniform bulk velocity and number density, after which the system was allowed to relax without forcing for several ion gyro periods.

Figure 2 shows comparisons between Vlasiator and WHAMP (Ronnmark 1983). WHAMP solves linearized analytic dispersion equations of waves in magnetized plasmas. A very close match is obtained with analytical solution for quasi-parallel wave propagation, and with WHAMP for quasi-perpendicular propagation. As Vlasiator and WHAMP solve Vlasov's equation using different approaches, namely hybrid-Vlasov simulation and linearized kinetic theory, the good correspondence is an indicator of the excellent numerical accuracy of Vlasiator. The non-propagating mode at ω_{ci} in right hand panel of Fig. 2, and its first harmonic, are due to the initial random perturbations fluctuating at the ion gyro frequency throughout the simulation box.

5. Results: Global Magnetospheric Simulations

Plasma processes occurring near Earth's bow shock were studied with spatially two-dimensional simulations (Pokhotelov et al. 2013). The dayside part of the magnetosheath, the bow shock, and the foreshock region were included in simulation domain. Nominal solar wind values were used, i.e., a Maxwellian ion distribution at 10^5 K temperature, 10^6 m^{-3} number density, 500 km/s bulk speed, and 5 nT magnetic field pointing at 45° Parker spiral angle. Earth's magnetic dipole points to the z direction, and has a strength of $8 \cdot 10^{22}$ Am^2. A 450×900 spatial mesh was used with $0.13\,R_E$ resolution, where R_E is the Earth radius. The velocity mesh limits were set to ± 2000 km/s in all directions with a resolution of 20 km/s. The resolution is sufficient to resolve ion thermal speeds of 65 km/s in the foreshock and 200 km/s in the magnetosheath. However, no attempt was made in trying to resolve thermal gyroscales of ~ 200 km.

After initial perturbations settle, a collisionless bow shock forms in front of the Earth (see Fig.3). The bow shock can be separated into quasi-parallel and quasi-perpendicular regions. Foreshock forms only in the quasi-parallel region, where ions are reflected off the bow shock back to the solar wind. The solar wind core is indicated by the small spheres in panels B-D in Fig.3. Ion distributions are qualitatively consistent with known single- and multi-spacecraft foreshock measurements. Distributions can be described as "narrow gyrating" near the foreshock boundary, "cap-shaped" deeper in the foreshock, and "diffuse cap" further towards the magnetotail (panels B,D,C in Fig.3). Reflected ions are unstable to wave generation, and drive quasi-monochromatic compressional oscillations with roughly 30 second period and $1-2R_E$ wavelength, with an amplitude of 5-10% of the ambient magnetic field and density, in the region where intermediate ion distributions are seen. These values are consistent with theoretical predictions for fast magnetosonic waves in the ideal MHD limit.

Magnetosheath is the region downstream of the bow shock. The solar wind is significantly thermalized and heated at the bow shock. The ion distributions change from "horseshoe" distributions, seen downstream of the bow shock, to gyrotropic bi-Maxwellian distributions (panel A of Fig.3) deeper inside the magnetosheath. Bi-Maxwellian distributions, with temperature anisotropy transverse to the ambient magnetic field direction, are known to be subject to mirror mode and ion-cyclotron instabilities. Vlasiator results clearly show signatures associated with perturbations induced by the mirror mode instability, i.e., anticorrelation between plasma density and magnetic field magnitude, loss cone ion distributions due to ion trapping between magnetic mirrors, and spatial lengthscales of the order of few ion inertial lengths.

Acknowledgments. The Vlasiator project has been supported by European Research Council under the European Community's 7th framework programme (FP-7/ 2007-2013/ ERC) agreement no. 200141-QuESpace. Results presented here were obtained by using computing resources granted by Partnership for Advanced Computing in Europe (PRACE). Authors also acknowledge the Academy of Finland for support.

References

Balsara, D. S., Rumpf, T., Dumbser, M., & Munz, C.-D. 2009, J. Comp. Phys., 228, 2480
Daldorff, L. K. S., Tóth, G., Gombosi, et al. 2014, J. Comp. Phys., 268, 236
Honkonen, I., von Alfthan, S., Sandroos, A., et al. 2013, Comp. Phys. Comm., 184, 1297
Janhunen, P., Palmroth, M., Laitinen, T., et al. 2012, J. Atmos. Sol.-Terr. Phys., 80, 48
Kempf, Y., Pokhotelov, D., von Alfthan, S., et al. 2013, Phys. Plasmas, 20, 112114
Langseth, J. O., & Leveque, R. J. 2000, J. Comp. Phys., 165, 126
Leveque, R. 1997, J. Comp. Phys, 131, 327
Londrillo, P., & del Zanna, L. 2004, J. Comp. Phys., 195, 17
Palmroth, M., Honkonen, I., Sandroos, A., et al. 2013, J. Atmos. Sol.-Terr. Phys., 99, 41
Pokhotelov, D., von Alfthan, S., Kempf, Y., et al. 2013, Ann. Geophys., 31, 2207

Ronnmark, K. 1983, Plasma Phys., 25, 699
Sandroos, A., Honkonen, I., von Alfthan, S., & Palmroth, M. 2013, Par. Comp., 39, 306
Savoini, P., Lembege, B., & Stienlet, J. 2013, J. Geophys. Res., 118, 1132
von Alfthan, S., Pokhotelov, D., Kempf, Y., et al. 2014, J. Atmos. Sol.-Terr. Phys., 120, 24

Part VI

Data Handling and Visualization